analytical chemistry

Article

Cite This: Anal. Chem. 2019, 91, 3710−3716

pubs.acs.org/ac

Electrochemiluminescence Enhanced by Restriction of Intramolecular Motions (RIM): Tetraphenylethylene Microcrystals as a Novel Emitter for Mucin 1 Detection

Ming-Hui Jiang, Sheng-Kai Li, Xia Zhong, Wen-Bin Liang, Ya-Qin Chai, Ying Zhuo,* and Ruo Yuan

Key Laboratory of Luminescent and Real-Time Analytical Chemistry (Southwest University), Ministry of Education, College of Chemistry and Chemical Engineering, Southwest University, Chongqing 400715, People's Republic of China

Supporting Information

ABSTRACT: Apart from the reported energy transfer mechanism of aggregation-induced electrochemiluminescence (AI-ECL) enhancement, a new strategy named restriction of intramolecular motions-driven ECL (RIM-ECL) enhancement is first proposed based on the phenomenon of a very strong electrochemiluminescence observed on the hexagonal tetraphenylethylene microcrystals (TPE MCs) in aqueous solution. Compared to TPE in molecule-isolation state with faint ECL, TPE in aggregate state (TPE MCs) showed a significantly enhanced ECL that was due to the restriction of intramolecular motions (RIM). Inspired by the unique luminescence characteristic of TPE MCs, we integrated the novel ECL emitter of TPE MCs and target-activated bipedal DNA walker together to fabricate a sensitive "off-on" ECL biosensor for Mucin 1 (MUC1) assay, which exhibited desirable linear response for a concentration scope from 1 fg/mL to 1 ng/mL with a low detection limit of 0.29 fg/mL. The RIM enhanced ECL demonstrated by the TPE MCs provides a new chapter in the exploration of aggregated organic emitters for further applications.

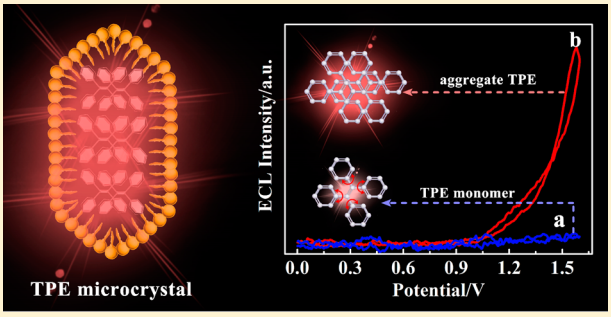

Over the past few years, the polycyclic aromatic hydrocarbons (PAHs)[1,2] have been considered to be a hot spot, because of their inexpensive production, structural tailorability, and excellent optoelectronic properties. These inherent superiorities drew tremendous interest for the potential applications of PAHs in diverse research fields such as advanced organic devices, biosensors, materials science, and asymmetric catalysis.[3−6] Among them, the electrochemiluminescence (ECL)[7] properties of PAHs (such as 9,10-diphenylanthracene (DPA), perylene, rubrene (Rub), phenanthrene derivatives)[8−10] were particularly eye-catching, since the systemic study of ECL was reported in 1964.[11] Moreover, these PAHs emitters were investigated usually in the organic phase, where the molecule is free in solution. Therefore, there was almost a blind area for the ECL mechanisms of PAHs in the aggregate state.

Very recently, a fantastic concept of aggregation-induced electrochemiluminescence (AI-ECL) debuted in 2017, where supramolecular aggregates based on the assemblies of square-planar Pt(II) complexes exhibited a stronger ECL emission, compared to that of its monomers.[12] Subsequently, Qi's group[13] synthesized an organic nanoparticles with the AI-ECL phenomenon, and the enhancement was ascribed to the energy transfer between donor and acceptor. Similarly, Sun et al.[14] also reported AI-ECL-enhanced polymer dots (Pdots) that were due to the resonance energy transfer between two different polymers. To date, the reason why AI-ECL was achieved was attributed to the energy transfer mechanism, where the emitter consisted of two molecules acting as the acceptor and the donor. Here, a significantly enhanced anodic ECL emission was first observed in the hexagonal tetraphenylethylene microcrystals (TPE MCs, as a aggregate state of TPE molecule). It was noticeable that this enhancement cannot be explained by the energy transfer mechanism, because of the absence of donor and acceptor in the TPE molecule. More concretely, from the analysis of its structure, the four phenyl rings with propeller-like conformation in TPE could freely rotate in molecule-isolation state, which might consume the energy via nonradiative relaxation pathways. And yet, these intermolecular motions were limited in the TPE MCs, suppressing nonradiative decay channels and making excited states radiatively relax.[15] This fact provided a theoretical basis for the ECL enhancement of TPE MCs, in comparison with that of the TPE in molecule-isolation state. Thus, for this unprecedented phenomenon, we have coined the term "restriction of intramolecular motions-driven ECL" (RIM-ECL) for the TPE MCs.

Mucin 1 (MUC1), which is a transmembrane glycoprotein that is overexpressed in most human malignancies, is regarded as a predominant biomarker for cancer. Accordingly, the

Received: December 27, 2018
Accepted: February 6, 2019
Published: February 6, 2019

DOI: 10.1021/acs.analchem.8b05949
Anal. Chem. 2019, 91, 3710−3716

Scheme 1. Preparation Processes of (A) the TPE MCs, (B) the Fabrication of the Proposed Biosensor, and (C) the Possible Luminescence Mechanism of the TPE MCs

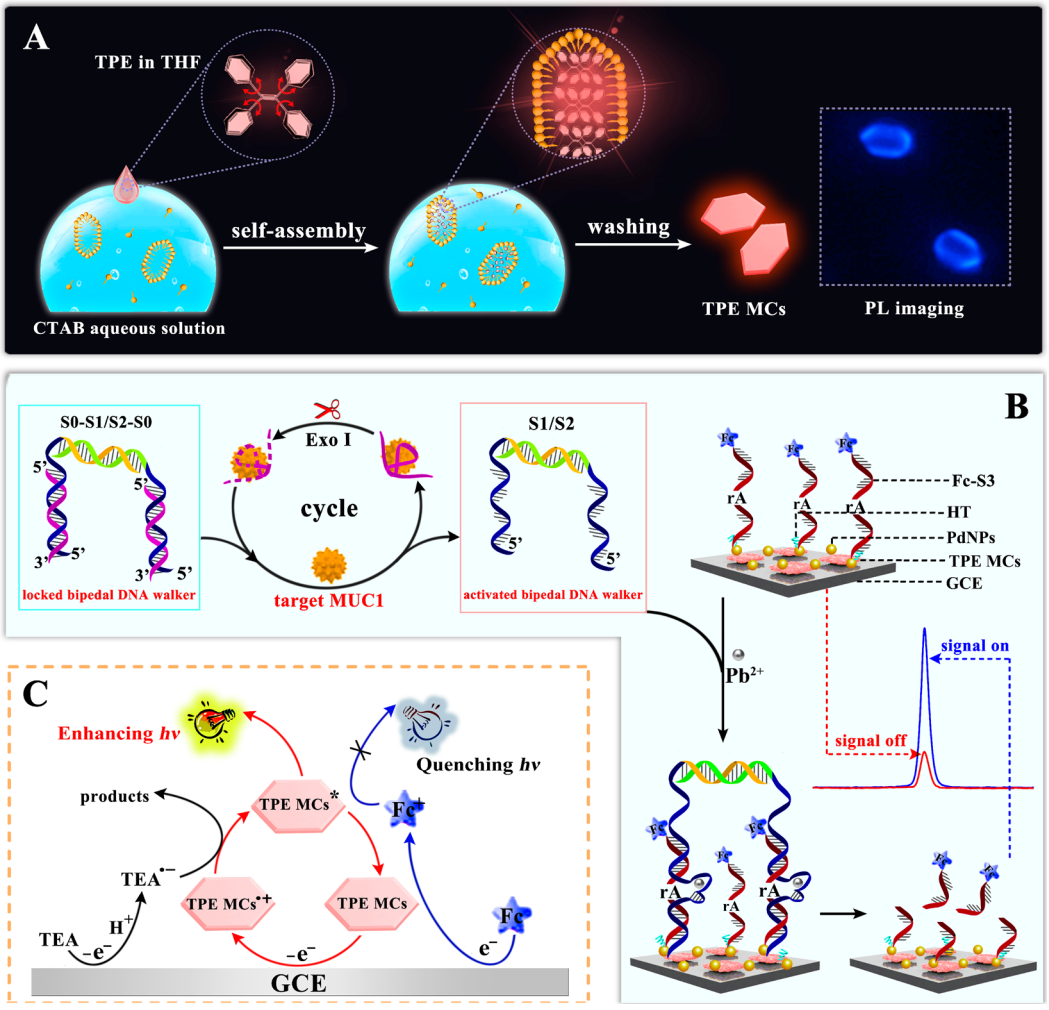

detection and quantification of MUC1 are of far-reaching significance in the early diagnostics of cancer. In this work, the TPE MCs, as a new type of ECL emitter, was used to developed an ultrasensitive "off−on" ECL biosensor for MUC1 assay with target-activated bipedal DNA walker as a signal switch. Originally, as depicted in Scheme 1A, the TPE MCs were synthesized by a surfactant-assisted self-assembly method and immobilized on the surface of working electrode to obtain a remarkably strong ECL signal in the presence of triethylamine (TEA). Besides, the palladium nanospheres (Pd NPs) were uniformly deposited onto the above modified electrode via electrostatic attraction for further assembling the Fc-labeled substrate DNA (Fc-S3), to build an ECL "signal-off" state. As demonstrated in Scheme 1B, with the help of Exo I,[16,17] the target-induced cyclic enzymatic amplification (TICEA) process was implemented to make the locked bipedal DNA walker (S0−S1/S2-S0) active and output numerous double-stranded DNA (S1/S2). Then, the S1/S2 was introduced to the surface of modified electrode and hybridized with the Fc-S3. As expected, upon addition of the cofactor Pb^{2+}, the DNAzymes[18] in S1/S2 cleaved the Fc-S3 into two parts, liberating the Fc-labeled DNA fragment from the electrode interface to solution. Meanwhile, the "feet" of S1/S2 were released to hybridize with other complementary Fc-S3 and then to repeat the above cleaving processes. As a result, the vast majority of Fc molecules were removed and a remarkable ECL signal was obtained as "signal-on" state. Because of the intense ECL emission of TPE MCs and the efficient "off−on" ECL switch platform, the developed biosensor could accomplish the sensitive detection of target MUC1 within a short period of time. Significantly, the finding of RIM-ECL enhancement process opened a new insight for the preparation of highly efficient ECL emitters and also for the deeper understanding about the luminescence mechanisms of PAHs.

EXPERIMENTAL SECTION

Preparation of the Hexagonal Tetraphenylethylene Microcrystals. The hexagonal tetraphenylethylene microcrystals (TPE MCs) were synthesized through the surfactant-assisted self-assembly method[19] with some modifications. First, 3 mg of TPE powder was dissolved in 1 mL THF solution and sonicated in an ultrasonic bath for 5 min. Following that, the resultant colorless solution was transferred into 10 mL of CTAB solution (10 mM) with moderately stirring for 20 min. The white products then were separated via centrifugation (11 000 rpm, 15 min at 4 °C) and further purified by washing 4 times with ultrapure water. Ultimately, the collected products were dried in the vacuum for subsequent use.

Synthesis of the Palladium Nanospheres. The palladium nanospheres (Pd NPs) were synthesized on the

DOI: 10.1021/acs.analchem.8b05949
Anal. Chem. 2019, 91, 3710−3716

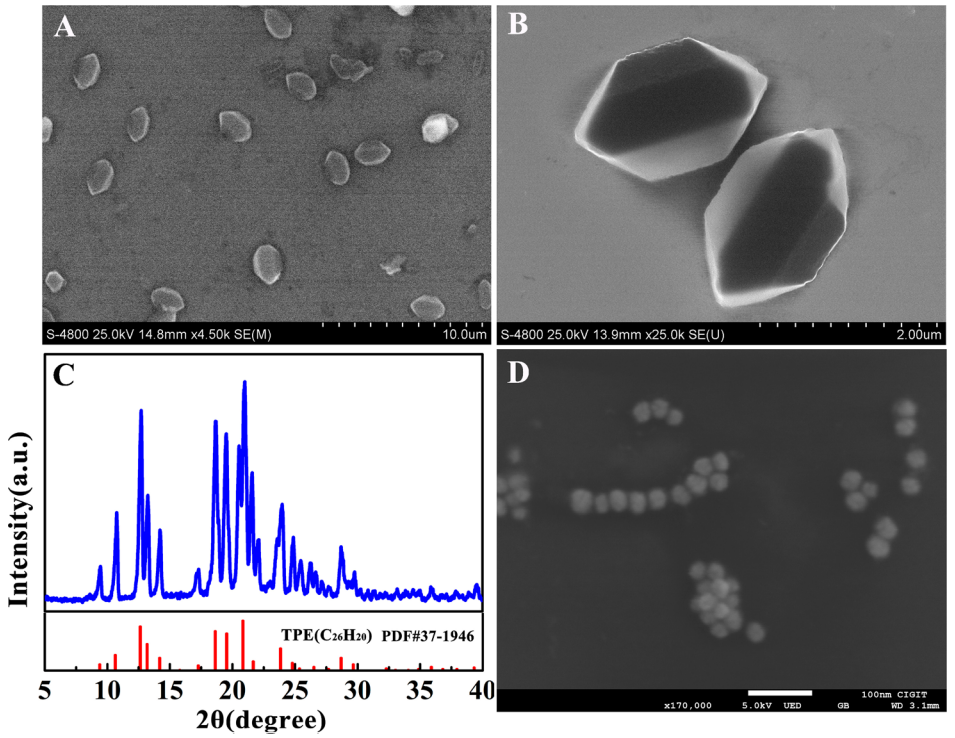

Figure 1. SEM images of (A) the TPE MCs, (B) the locally enlarged TPE MCs, and (D) the Pd NPs. Panel (C) shows the XRD pattern of the TPE MCs.

basis of the previous study[20] with minor modification. At first, the Pd seeds must be formed to act as building blocks. Briefly, 10 mL of CTAC solution (0.1 M) and 0.05 mL of K_2PdCl_4 solution (0.05 M) were mixed at room temperature. Then, 0.1 mL of freshly prepared ice-cold $NaBH_4$ solution (0.1 M) was rapidly injected into the above solution under slight stirring. To decompose the excessive $NaBH_4$, the resultant Pd seeds were aged for 3 h in darkness. Subsequently, 0.1 mL of the prepared Pd seeds and 5 mL of CTAC solution (0.01 M) were transferred into 3 mL of K_2PdCl_4 solution (0.001 M) with moderately stirring. Following that, 0.1 mL of fresh AA solution (0.1 M) was promptly added into the above mixed solution and kept for 15 min. The products then were collected by centrifugation (11 000 rpm, 15 min) and washed with ultrapure water three times. In the end, the resultant Pd NPs were redispersed in 5 mL of ultrapure water for subsequent experiments.

Fabrication of the Proposed Biosensor. As shown in Scheme 1B, the bare GCE (Φ = 4 mm) was first polished with 0.3 and 0.05 μm alumina powder successively, following the sonication process in anhydrous ethanol and ultrapure water to obtain a clean electrode surface.[21] Then, 10 μL of TPE MCs was deposited dropwise on the pretreated GCE and dried in air to get a uniform layer. Afterward, 10 μL of Pd NPs was coated on the modified electrode (TPE MCs/GCE) to form a well-dispersed Pd NPs layer based on the electrostatic attraction (the corresponding zeta potential values of TPE MCs and Pd NPs were shown in section S1.3 in the Supporting Information). Then, 10 μL of Fc-labeled substrate DNA (Fc-S3, 2.0 μM) solution was placed onto the surface of modified electrode (Pd NPs/TPE MCs/GCE) and maintained at 4 °C overnight. After being thoroughly rinsed with PBS (0.1 M, pH 7.4), the above modified electrode (Fc-S3/Pd NPs/TPE MCs/GCE) was incubated with 10 μL of HT (1.0 mM) solution for 1 h at room temperature to block physically adsorbed effects. Ultimately, the prepared biosensor (HT/Fc-S3/Pd NPs/TPE MCs/GCE) was placed in 4 °C for the following use (the CV and ECL characterizations were performed to prove the successful construction of biosensor in section S1.7 in the Supporting Information).

Operating Principle of the Bipedal DNA Walker. As illustrated in Scheme 1B, the S1/S2 presented here was operated on the functionalized sensing interface with a good deal of Fc-S3 (ECL "signal-off" state). To accomplish this, the S0−S1/S2−S0 was first formed via annealing the mixture of S1, S2, and S0. Notably, the S1 and S2 were designed to contain three functional sequence: (1) the mutual hybridization region for S1 and S2 to form the rigid DNA duplex torso. (2) the polythymine spacer (T15) acted as the swing arm to avoid the steric hindered effect. (3) the Pb^{2+}-dependent DNAzyme strand with a catalytic center and two recognition arms, which can cleave RNA in specific substrate DNAs. Accordingly, the S1/S2 was composed of a rigid DNA duplex domain as "body" and two flexible single-stranded regions as its double "feet". Initially, the two identical DNAzyme strands in DNA walker were blocked through the partial hybridization with S0. After the introduction of target MUC1, the S0 were taken away from S0−S1/S2−S0 by the specific binding of MUC1-aptamer, outputting the S1/S2. Meanwhile, in virtue of Exo I with digestion function, the S0 was hydrolyzed into mononucleotides from the 3′-terminus to 5′-terminus direction, releasing the MUC1 to bind with remaining S0 and realizing the circulation of MUC1. Subsequently, the S1/S2 was brought close to the sensing interface and hybridized with the Fc-S3. Upon addition of the cofactor Pb^{2+}, the DNAzymes in S1/S2 cleaved the Fc-S3 into two parts, liberating the Fc-labeled DNA fragment from the electrode interface to solution. Meanwhile, the "feet" of S1/S2 were

DOI: 10.1021/acs.analchem.8b05949
Anal. Chem. 2019, 91, 3710−3716

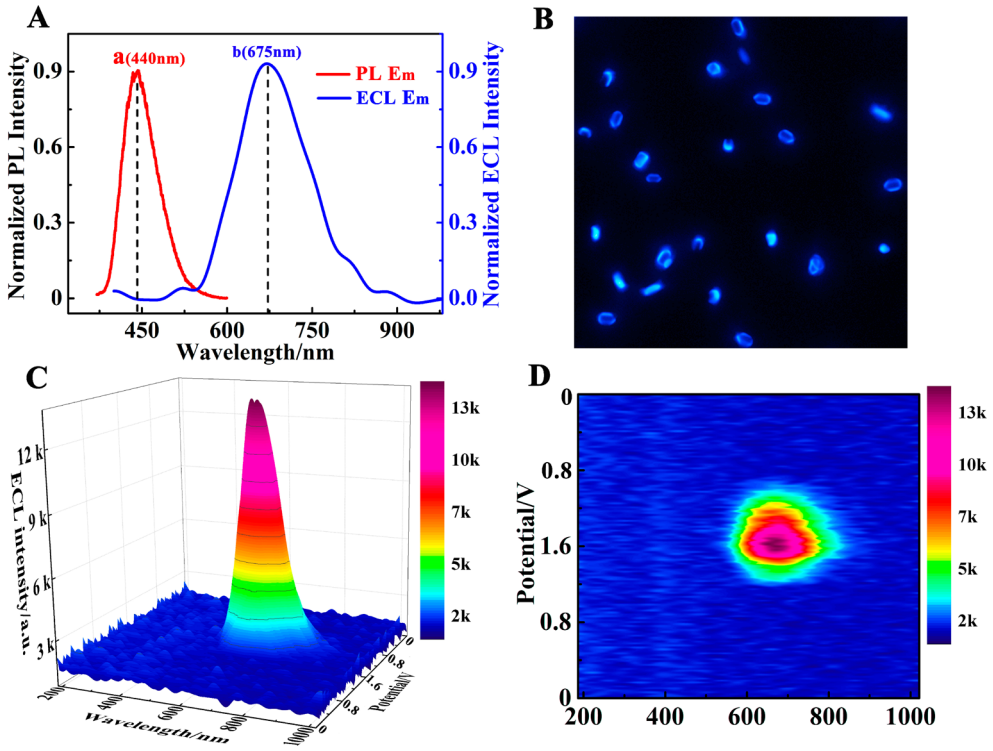

Figure 2. (A) Normalized PL (λ_{ex} = 356 nm) emission spectrum (curve a) and ECL emission spectrum (curve b) of the TPE MCs. (B) Fluorescence microscopic image of the TPE MCs. (C) 3D color map surface and (D) heat map image of ECL from the TPE MCs.

released to hybridize with other complementary Fc-S3 and then to repeat the above cleaving processes. In principle, the S1/S2 could pass through the entire sensing interface until a vast majority of Fc molecules were removed, after which would complete the recovery of ECL signal ("signal-on" state). The polyacrylamide gel electrophoresis (PAGE) analysis was implemented to confirm this feasibility, and the result was shown in section S1.8 in the Supporting Information.

Preparation of the Target-Activated Bipedal DNA Walker (S1/S2). At first, in order to obtain the locked bipedal DNA walker (S0−S1/S2−S0), the mixture of 2 μM DNAzyme strand 1 (S1), 2 μM DNAzyme strand 2 (S2), and 5 μM aptamer strand of MUC1 (S0) in Tris-HCl buffer were annealed at 95 °C for 10 min and then cooled to room temperature at a rate of 1 °C/min. The target-induced cyclic enzymatic amplification (TICEA) then proceeded in a microcentrifuge tube. In brief, 100 μL of 1 × Exo I digestion reaction buffer containing 1 μM S0−S1/S2−S0, MUC1 with different concentrations and 1 U/μL Exo I were incubated at 37 °C for 90 min, followed by a heating process at 80 °C for 20 min to terminate the digestion reaction of Exo I. The resultant reaction solution containing S1/S2 was obtained for further use.

Measurement Procedure. For ECL detection, 10 μL of the resultant S1/S2 solution and 2 μL of Pb^{2+} solution (6 mM) were first deposited dropwise on the surface of fabricated biosensor and incubated at 37 °C for 90 min to trigger the walking of DNA walker. Subsequently, the biosensor was rinsed thoroughly with ultrapure water, and the ECL signal measurement was completed by a MPI-A ECL analyzer in 0.1 M PBS (pH 7.4) containing 20 mM TEA. Also, the scanning potential ranged from 0 to 1.6 V, with a scan rate of 300 mV/s.

RESULTS AND DISCUSSION

SEM and XRD Characterization of the Nanomaterials. The morphologies and microstructure of the synthesized nanomaterials in this work were characterizated by scanning electron microscopy (SEM) and X-ray diffraction (XRD) techniques, respectively. As displayed in Figure 1A, the TPE MCs exhibited a well-defined shape of irregular hexagonal structure with a uniform size (~2 μm). Figure 1B showed a locally enlarged SEM image, in which the smooth surface of TPE MCs was observed clearly. In order to further prove the microstructures of TPE MCs, XRD spectra of the TPE MCs were recorded by an X-ray diffractometer (Model XD-3) in a 2θ range from 5° to 40° with a scanning rate of 4°/min. From Figure 1C, the characteristic diffraction peaks of TPE MCs were clearly exhibited and in good agreement with the standard spectrum database (JCPDS No. 37-1946), confirming the formation of a crystal structure in TPE MCs. In addition, Figure 1D clearly illustrated the SEM images of the Pd NPs with a relatively uniform size of 20 nm, and their surfaces were extremely rough, which manifested that the Pd NPs might possess abundant active site.

Optical Properties of TPE MCs. Optical properties of the prepared TPE MCs were investigated by photoluminescence (PL) and ECL spectra, respectively. As shown in Figure 2A, the strongest PL emission peak of TPE MCs was observed at 440 nm (curve a) by setting up the optimal excitation wavelength at 356 nm. In addition, from the fluorescence imaging photograph in Figure 2B, the TPE MCs presented a bright blue luminescence under the excitation wavelength of 488 nm and its profile was in good agreement with the aforementioned SEM imaging. Meanwhile, the ECL spectra of TPE MCs was investigated based on our recently introduced spectrograph with a time gap of 0.1 s during one potential scan from 0 to 1.6 V and then back to 0 V. The three-dimensional

DOI: 10.1021/acs.analchem.8b05949
Anal. Chem. 2019, 91, 3710−3716

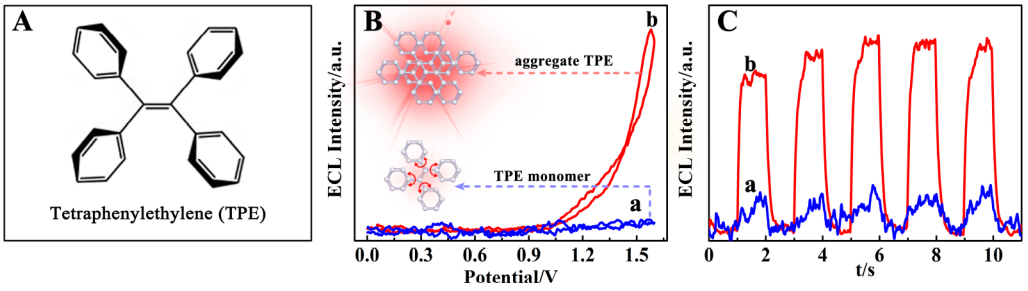

Figure 3. (A) Structure of the TPE molecular. (B) ECL-potential profile for bare GCE in 0.1 M $TBAPF_6$ THF solution containing 1 mg/mL TPE monomers and 20 mM TEA (curve a), and in 0.1 M PBS containing 1 mg/mL TPE MCs and 20 mM TEA (curve b). The inset of panel (B) shows a schematic diagram of the relationship between emission intensity and molecular states for the TPE. (C) ECL transients obtained for bare GCE in 0.1 M $TBAPF_6$ THF solution containing 1 mg/mL TPE monomers and 20 mM TEA (trace (a)), and 0.1 M PBS containing 1 mg/mL TPE MCs and 20 mM TEA by stepping the potential between 0 and 1.6 V (trace (b)).

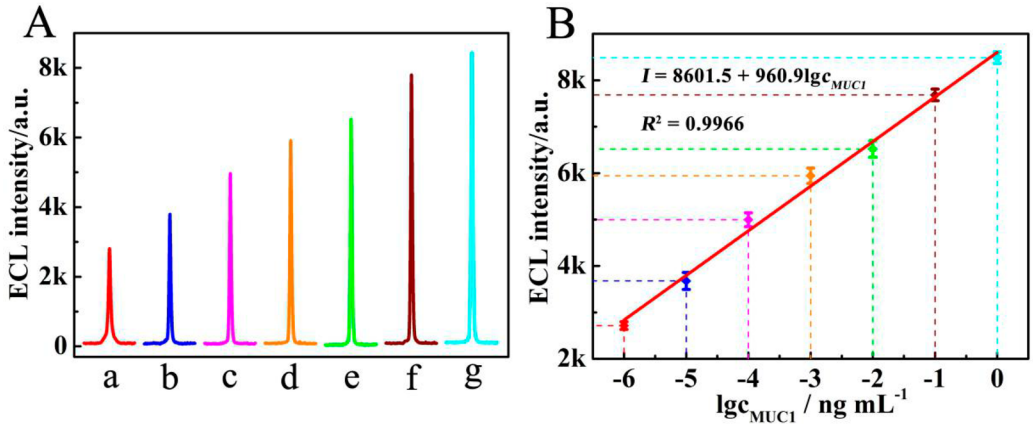

Figure 4. (A) ECL responses of the developed biosensor incubated with different MUC1 concentrations: (a) 1 fg/mL, (b) 10 fg/mL, (c) 100 fg/mL, (d) 1 pg/mL, (e) 10 pg/mL, (f) 100 pg/mL, and (g) 1 ng/mL. (B) Calibration plot for the ECL intensity versus the logarithm of the MUC1 concentration.

(3D) color map surface (Figure 2C) traced the evolution and devolution process of the TPE MCs ECL emission and provided a new view of the ECL properties. Furthermore, to observe the ECL emission wavelength of TPE MCs intuitively, a typical heat map image of ECL from the TPE MCs is shown in Figure 2D, with maximum emission wavelength at 675 nm. Noticeably, there was an apparent red shift by almost 235 nm between the ECL and PL emission spectrum of TPE MCs. The similar phenomenon was also observed in other organic luminophores,[22,23] which implied that the formation of excited dimer might be a highly favorable pathway for ECL radiation process. In addition, the comparison of the Raman spectra of the free TPE monomers and aggregate TPE MCs was demonstrated in section S1.5 in the Supporting Information, where much weaker C−H in-plane bending vibrational modes were observed in TPE MCs.

RIM-ECL Strategy Investigation of the TPE. Tetraphenylethylene (TPE), which is a nonplanar propeller-shaped molecule, consists of a olefinic stator and four phenyl rotors (Figure 3A). In organic phase (THF), the TPE was dissolved as molecule-isolation state, in which the four phenyl rotors could freely motion against the olefinic stator by single-bond axes. Basic physics tells us that any intramolecular motions will consume energy, thereby weakening or even eliminating the radiative emissions of the molecule. However, in aqueous solution, the TPE was completely insoluble and had a tendency to aggregate in an incompact and amorphous manner,[24] thanks to the steric effect between the moving phenyl rotors. Therefore, we speculated that the restriction of intramolecular motions (RIM) was a major cause for the ECL enhancement. To confirm the validity of this speculation, the ECL-potential and ECL-transient curves of TPE/TEA system were investigated in organic electrolyte and in PBS (pH 7.4), respectively. As displayed in Figure 3B, almost no ECL signal (curve a) was observed for TPE monomers (1 mg/mL) in $TBAPF_6$ THF solution containing 20 mM TEA as a coreactant. The reason might be the intramolecular motions transformed the photonic energy into heat and annihilated its excited state nonradiatively to render the TPE nonemissive. Surprisingly, the TPE MCs (1 mg/mL) dispersed in PBS exhibited a significantly enhanced ECL emission (curve b), compared to that in $TBAPF_6$ THF solution. The reason might be that the RIM caused by the physical constraint suppressed the nonradiative decay, opened up the radiative channel, and lowered the electronic energy level. Moreover, the ECL-transients spectra of TPE in different electrolyte solutions were obtained via the step pulse method with a pulse potential between 0 and 1.6 V (pulse time of 1s). As seen in Figure 3C, when the TPE MCs was dispersed in PBS, a series of ECL peaks (curve b) were markedly enhanced, compared to that of TPE monomers dissolved in $TBAPF_6$ THF solution (curve a). Furthermore, the ECL relative quantum efficiency obtained on the TPE MCs/TEA system in PBS was ~12.7 times higher than that of TPE monomers/TEA system in $TBAPF_6$ THF solution. (See section S1.4 in the Supporting Information for details.) These results of the ECL-potential and ECL-transients

DOI: 10.1021/acs.analchem.8b05949
Anal. Chem. 2019, 91, 3710−3716

tests consistently demonstrated the rationality of the preceding hypothesis, that is, the RIM of TPE MCs caused a dominant contribution to the ECL enhancement.

ECL Responses of the Proposed Biosensor toward MUC1. Based on the optimized reaction conditions (the experimental optimizations were displayed in section S1.6 in the Supporting Information), the sensitivity of the proposed biosensor was evaluated through monitoring the ECL response of the biosensor to different concentrations of MUC1. As exhibited in Figure 4A, the ECL signal enhanced gradually with the increase of MUC1 concentrations (1 fg/mL to 1 ng/mL). In addition, Figure 4B displayed the corresponding calibration plot, from which we could clearly see an outstanding linear relationship between the ECL intensities and the logarithmic value of MUC1 concentrations. The regression equation was $I = 8601.5 + 960.9 \log c_{MUC1}$ with a squared correlation coefficient of $R^2 = 0.9966$. According to the 3σ rule,[25] a detection limit of 0.29 fg/mL for the biosensor could be estimated, which showed a superior detection sensitivity. Moreover, the comparison between the developed MUC1 detection method and previous reports are displayed in Table 1.

Table 1. Comparison of MUC1 Detection Based on Different Methods

method	detection range	detection limit	ref
fluorescence	0.001–20 ng/mL	0.23 pg/mL	26
EC	from 1.0 nM to 1.0 μM	0.827 nM	27
ECL	10^{-3}–10^{3} pg/mL	0.62 fg/mL	28
ECL	10^{-3}–10^{4} pg/mL	0.23 fg/mL	29
ECL	10^{-3}–10^{3} pg/mL	0.29 fg/mL	this work

Selectivity and Stability of the MUC1 Biosensor. At the same time, the selectivity and stability, as important performances of the proposed biosensor, were investigated. First, two interfering proteins including CEA and AFP (1 ng/mL), which existed in healthy human serum at high concentrations (ng/mL levels), were selected artificially to execute comparative experiments to evaluate the selectivity of the biosensor. According to Figure 5A, the developed biosensor with above interfering proteins displayed low ECL signal, which were almost the same as that of the blank solution. Furthermore, the ECL responses of the biosensor incubated with a mixture (1 ng/mL of CEA and AFP, 100 pg/mL of MUC1) remained similar to that of the MUC1 solution (100 pg/mL). These results manifested that the proposed biosensor held good selectivity for MUC1 detection. Subsequently, to assess the stability of the biosensor, the consecutive ECL scans of 15 cycles were monitored by using 1 ng/mL MUC1 as a model. There was no obvious fluctuation (RSD = 1.07%) of the ECL peak intensity in Figure 5B, demonstrating the satisfactory stability of the obtained biosensor.

Detection of the MUC1 in Human Serum. The standard addition method-based recovery experiments were performed to assess the feasibility of the proposed biosensor for the MUC1 detection. Briefly, the whole blood samples from healthy human (supported by Xinqiao Hospital of Army Medical University, China) were centrifuged for 20 min with 3500 rpm to obtain human serum, and then the purified human serum was diluted to 50-fold with PBS (pH 7.4) for the preparation of various concentrations MUC1. As listed in Table 2, the recovery varied from 91.2% to 117%, which suggested that the proposed biosensor endowed prominent potential for clinical diagnosis.

Table 2. Recovery Results for MUC1 Determination Indiluted Human Serum Samples

sample	added (pg mL^{-1})	found (pg mL^{-1})	RSD (%)	recovery (%)
1	0.01	0.00912	2.7	91.2
2	0.1	0.106	4.1	106
3	1	0.977	2.1	97.7
4	10	11.6	1.1	116
5	100	117	2.3	117

CONCLUSION

In summary, not only was the anodic ECL behavior of TPE MCs prepared by the self-assembly method observed in aqueous media for the first time, but a dramatically increased ECL signal also was achieved, in comparison with that of dispersed molecules in organic solution. We coined the unique phenomenon as RIM-ECL enhancement, which contributed to an in-depth understanding for the ECL mechanisms of PAHs in aqueous solution. With the magical TPE MCs as ECL beacon, the proposed biosensor accomplished sensitive

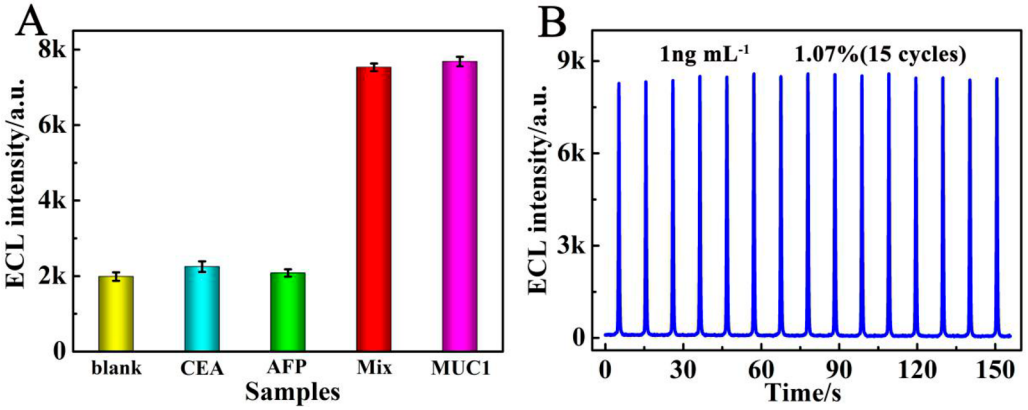

Figure 5. (A) Selectivity of the developed biosensor toward other interfering proteins (1 ng/mL). (B) Stability assessment of the developed biosensor by continuous scanning for 15 cycles.

DOI: 10.1021/acs.analchem.8b05949
Anal. Chem. 2019, 91, 3710–3716

detection for target MUC1. In view of the reported results, this work has enabled us to "visit" scenery that we have previously never seen in the field of ultrasensitive bioanalysis.

■ ASSOCIATED CONTENT

Supporting Information

The Supporting Information is available free of charge on the ACS Publications website at DOI: 10.1021/acs.analchem.8b05949.

Reagents and material, apparatus, zeta potential measurement of particles, the ECL relative quantum efficiency of TPE, Raman spectra of the free TPE monomers and aggregate TPE MCs, optimization of the experimental conditions, CV and ECL characterizations of the proposed biosensor and polyacrylamide gel electrophoresis (PAGE) analysis (DOC)

■ AUTHOR INFORMATION

Corresponding Author

*Tel.: +86 23 68253172. Fax: +86 23 68253172. E- mail: yingzhuo@swu.edu.cn.

ORCID

Ya-Qin Chai: 0000-0003-4392-9592

Ying Zhuo: 0000-0002-4491-1186

Ruo Yuan: 0000-0003-3664-6236

Notes

The authors declare no competing financial interest.

■ ACKNOWLEDGMENTS

This work was financially supported by the NNSF of China (Nos. 21675130, 21775124, 21575116, and 21675129), the Natural Science Foundation Project of CQ CSTC (No. cstc2018jcyjAX0546) and the Fundamental Research Funds for the Central Universities (No. XDJK2018AA003), China.

■ REFERENCES

(1) Ko, S. H.; Lee, T.; Park, H.; Ahn, D.; Kim, K.; Kwon, Y.; Cho, S. J.; Ryoo, R. *J. Am. Chem. Soc.* **2018**, *140*, 7101−7107.

(2) Ito, H.; Segawa, Y.; Murakami, K.; Itami, K. *J. Am. Chem. Soc.* **2019**, *141*, 3−10.

(3) Zhang, X.; Xu, Z. Q.; Si, W. L.; Oniwa, K.; Bao, M.; Yamamoto, Y.; Jin, T. N. *Nat. Commun.* **2017**, *8*, 15073.

(4) Li, H. Y.; Wang, C. F.; Hou, T.; Li, F. *Anal. Chem.* **2017**, *89*, 9100−9107.

(5) Xu, Y.; Zhang, Y. X.; Sugiyama, H.; Umano, T.; Osuga, H.; Tanaka, K. *J. Am. Chem. Soc.* **2004**, *126*, 6566−6567.

(6) Knowles, R. R.; Lin, S.; Jacobsen, E. N. *J. Am. Chem. Soc.* **2010**, *132*, 5030−5032.

(7) Zhang, P.; Jiang, J.; Yuan, R.; Zhuo, Y.; Chai, Y. Q. *J. Am. Chem. Soc.* **2018**, *140*, 9361−9364.

(8) Ritchie, E. L.; Pastore, P.; Wightman, R. M. *J. Am. Chem. Soc.* **1997**, *119*, 11920−11925.

(9) Dick, J. E.; Renault, C.; Kim, B. K.; Bard, A. J. *J. Am. Chem. Soc.* **2014**, *136*, 13546−13549.

(10) Qi, H. L.; Chen, Y. H.; Cheng, C. H.; Bard, A. J. *J. Am. Chem. Soc.* **2013**, *135*, 9041−9049.

(11) Hercules, D. M. *Science* **1964**, *145*, 808−809.

(12) Carrara, S.; Aliprandi, A.; Hogan, C. F.; De Cola, L. *J. Am. Chem. Soc.* **2017**, *139*, 14605−14610.

(13) Liu, H. W.; Wang, L. F.; Gao, H. F.; Qi, H. L.; Gao, Q.; Zhang, C. X. *ACS Appl. Mater. Interfaces* **2017**, *9*, 44324−44331.

(14) Sun, F.; Wang, Z. Y.; Feng, Y. Q.; Cheng, Y. X.; Ju, H. X.; Quan, Y. W. *Biosens. Bioelectron.* **2018**, *100*, 28−34.

(15) Feng, H. T.; Yuan, Y. X.; Xiong, J. B.; Zheng, Y. S.; Tang, B. Z. *Chem. Soc. Rev.* **2018**, *47*, 7452−7476.

(16) Wu, Z.; Zhen, Z.; Jiang, J. H.; Shen, G. L.; Yu, R. Q. *J. Am. Chem. Soc.* **2009**, *131*, 12325−12332.

(17) Jiang, X. Y.; Wang, H. J.; Wang, H. J.; Yuan, R.; Chai, Y. Q. *Anal. Chem.* **2016**, *88*, 9243−9250.

(18) Fan, H. H.; Zhao, Z. L.; Yan, G. B.; Zhang, X. B.; Yang, C.; Meng, H. M.; Chen, Z.; Liu, H.; Tan, W. H. *Angew. Chem.* **2015**, *127*, 4883−4887.

(19) Cai, W. R.; Zhang, G. Y.; Lu, K. K.; Zeng, H. B.; Cosnier, S.; Zhang, X. J.; Shan, D. *ACS Appl. Mater. Interfaces* **2017**, *9*, 20904−20912.

(20) Zhang, L.; Zhang, J. W.; Jiang, Z. Y.; Xie, S. F.; Jin, M. S.; Han, X. G.; Kuang, Q.; Xie, Z. X.; Zheng, L. S. *J. Mater. Chem.* **2011**, *21*, 9620−9625.

(21) Zhou, Y.; Wang, H. J.; Zhang, H.; Chai, Y. Q.; Yuan, R. *Anal. Chem.* **2018**, *90*, 3543−3549.

(22) Debad, J. D.; Morris, J. C.; Lynch, V.; Magnus, P.; Bard, A. J. *J. Am. Chem. Soc.* **1996**, *118*, 2374−2379.

(23) Fabrizio, E. F.; Prieto, I.; Bard, A. J. *J. Am. Chem. Soc.* **2000**, *122*, 4996−4997.

(24) Zhao, X.; Zhou, W.; Lu, C. *Anal. Chem.* **2017**, *89*, 10078−10084.

(25) Dixit, C. K.; Vashist, S. K.; O'Neill, F. T.; O'Reilly, B.; MacCraith, B. D.; O'Kennedy, R. *Anal. Chem.* **2010**, *82*, 7049−7052.

(26) Yang, W. T.; Shen, Y.; Zhang, D. Y.; Xu, W. J. *Chem. Commun.* **2018**, *54*, 10195−10198.

(27) Deng, C. Y.; Pi, X. M.; Qian, P.; Chen, X. Q.; Wu, W. M.; Xiang, J. *Anal. Chem.* **2017**, *89*, 966−973.

(28) Jiang, X. Y.; Wang, H. J.; Wang, H. J.; Zhuo, Y.; Yuan, R.; Chai, Y. Q. *Anal. Chem.* **2017**, *89*, 4280−4286.

(29) Li, S. K.; Chen, A. Y.; Niu, X. X.; Liu, Z. T.; Du, M.; Chai, Y. Q.; Yuan, R.; Zhuo, Y. *Chem. Commun.* **2017**, *53*, 9624−9627.

DOI: 10.1021/acs.analchem.8b05949
Anal. Chem. 2019, 91, 3710−3716